Opt Quant Electron (2008) 40:991–1003
DOI 10.1007/s11082-009-9283-4

Complete analysis of photonic crystal fibers by full-vectorial 2D-FDTD method

K. Sheikhi · N. Granpayeh

Received: 3 November 2008 / Accepted: 24 February 2009 / Published online: 10 March 2009

Abstract In this paper, an extended finite difference time domain (FDTD) algorithm for the full-vectorial analysis of photonic crystal fibers has been derived. For achieving a good convergence and high accuracy, a kind of modified conformal FDTD method has been applied. An anisotropic perfectly matched layer for truncation of boundary conditions has been introduced. Material and chromatic dispersions are numerically investigated for the photonic crystal fibers with different dimensions and geometrical parameters and different dispersion behaviors are exhibited.

Keywords Finite-difference time-domain (FDTD) · Photonic crystal fibers (PCFs) · Chromatic dispersion

1 Introduction

Recently, photonic crystal fibers (PCFs) have been the matter of numerous researches and have been under vast analytical and numerical studies. This material although has made from undoped fused silica, it shows some especial properties which is inaccessible by conventional optical fibers. Their claddings consist of a number of air holes in the pure silica which runs along the fiber length. However, because of their complex transverse structure, special configuration and photonic band-gap (PBG) effect, analytical study of PCFs are so complicated and consequently numerical techniques to model PCFs fell into a deep consideration.

Photonic crystal fibers are categorized into two different kinds. The first one called index-guiding PCF, has a central part of fused silica surrounded by a regular hexagonal lattice of air holes working according to the total internal reflection law, the same as conventional optical fibers. The next one which is called photonic band-gap fiber (PBGF) has a periodic

K. Sheikhi (✉) · N. Granpayeh
Faculty of Electrical Engineering, K. N. Toosi University of Technology, Tehran, Iran
e-mail: sheikhi_k@ee.kntu.ac.ir

N. Granpayeh
e-mail: granpayeh@eetd.kntu.ac.ir

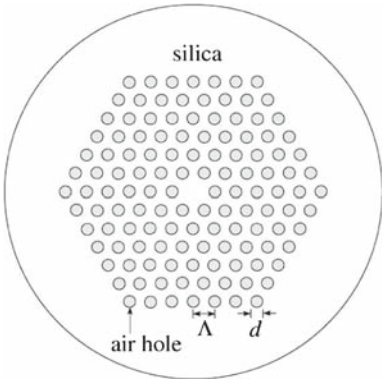

Fig. 1 Structure of the PCF under study

structure cladding and a lower index core which the guidance of light is possible only in the wavelength range of cladding photonic band-gap.

This paper focuses on the index-guiding fibers which are suitable for long haul communication systems and networks, the structure of which are shown in Fig. 1. In the next section the extended formulation of our detailed theoretical investigation is considered. Next, numerical results and accuracy of our method is exhibited and the paper is concluded. We have shown that our FDTD method used to analyze the PCFs in this project is straightforward and the requirements for the central processing unit (CPU) time and memory size are moderate compared to the other numerical methods such as finite element method (FEM). As the FDTD algorithm is based on an orthogonal, regular Cartesian lattice, it has a great challenge in the simulation of structures with cylindrical cross-sections. Hence, by using the modifications of Appendix A, this problem for the simulation of fibers has been dealt with thoroughly and the results show a great accuracy.

2 Theoretical formulation

Maxwell's equations in a nonmagnetic source free area can be written in the frequency domain as:

$$\vec{\nabla} \times \vec{E}(\omega) = -j\omega\mu_0 \vec{H}(\omega) \tag{1}$$

$$\vec{\nabla} \times \vec{H}(\omega) = j\omega\varepsilon_0\varepsilon_r(\omega)\vec{E}(\omega) \tag{2}$$

where, $\vec{E}$ and $\vec{H}$ are the electric and magnetic field, μ_0 and ε_0 are the permeability and permittivity in vacuum, respectively and ε_r is the relative permittivity of the medium.

The PCFs have a frequency dependent refractive index, the relation of which can be expressed by Sellmeier formula (Malitson 1965; Jiang et al. 2006) as:

$$n^2_{\text{silica}}(\omega) = \varepsilon_r(\omega) = 1 + \sum_{k=1}^{2} \frac{b_k \omega_k^2}{\omega_k^2 - \omega^2} \tag{3}$$

which covers the wavelength range of 0.5–2 μm and can model the chromatic dispersion of PCFs accurately. In this equation $b_1 = 1.1195$, $b_2 = 0.772443$, and $\omega_k = 2\pi c/\lambda_k (k = 1, 2$, c is the speed of light in vacuum, $\lambda_1 = 0.0896926\mu$m, and $\lambda_2 = 9.226961\mu$m).

By substitution of Eq. 3 in Eq. 2, we can write:

$$\vec{\nabla} \times \vec{H}(\omega) = j\omega\varepsilon_0 \vec{E}(\omega) + \vec{J}(\omega) \tag{4}$$

where:

$$\vec{J}(\omega) = j\omega\varepsilon_0 \sum_{k=1}^{2} \frac{b_k \omega_k^2}{\omega_k^2 - \omega^2} \vec{E}(\omega) \tag{5}$$

Equation 5, can be written as (Jiang et al. 2006):

$$\vec{J}(\omega) = \sum_{k=1}^{2} [\vec{J}_k^{+}(\omega) + \vec{J}_k^{-}(\omega)] \tag{6}$$

where:

$$\vec{J}_k^{\pm}(\omega) = -\frac{j\varepsilon_0}{2} b_k \frac{\omega_k^2}{\omega \pm \omega_k} \vec{E}(\omega) \tag{7}$$

Equations 6 and 7 can be transformed to time domain as:

$$\vec{J} = \sum_{k=1}^{2} [\vec{J}_k^{+} + \vec{J}_k^{-}] \tag{8}$$

and:

$$\frac{\partial \vec{J}_k^{\pm}}{\partial t} \pm j\omega_k \vec{J}_k^{\pm} = \frac{\varepsilon_0}{2} b_k \omega_k^2 \vec{E} \tag{9}$$

for $k = 1$ and 2.

Now, it is possible to introduce a set of Maxwell's equations in time domain for the FDTD simulation of the PCFs as follows:

$$\vec{\nabla} \times \vec{E} = -\mu_0 \frac{\partial \vec{H}}{\partial t} \tag{10}$$

$$\vec{\nabla} \times \vec{H} = \varepsilon_0 \frac{\partial \vec{E}}{\partial t} + \vec{J} \tag{11}$$

One of the greatest challenges of the FDTD method has been the efficient and accurate solution of electromagnetic wave interaction problems in unbounded regions. For such problems, a Perfectly Matched Layer (PML) as an absorbing boundary condition (ABC) must be introduced at the outer lattice boundary to simulate the extension of the lattice to infinity. We have used the Convolutional Perfectly Matched Layer (CPML[1]) as an APML for our FDTD boundary treatment, therefore, Eqs. 10 and 11 can be expressed as (Taflove and Hagness 2005):

[1] The CPML is based on the stretched-coordinate form of Berenger's PML and accommodates more general metric tensor coefficients that can lead to improved absorption of slowly varying evanescent waves. The CPML formulation is more accurate than the classical PMLs, more efficient and suitable for the application of domains with generalized materials.

$$\varepsilon_0 \frac{\partial E_x}{\partial t} + J_x = \left(\frac{1}{k_y}\frac{\partial H_z}{\partial y} - \frac{1}{k_z}\frac{\partial H_y}{\partial z}\right) + \left(\zeta_y * \frac{\partial H_z}{\partial y} - \zeta_z * \frac{\partial H_y}{\partial z}\right) \tag{12}$$

$$\varepsilon_0 \frac{\partial E_y}{\partial t} + J_y = \left(\frac{1}{k_z}\frac{\partial H_x}{\partial z} - \frac{1}{k_x}\frac{\partial H_z}{\partial x}\right) + \left(\zeta_z * \frac{\partial H_x}{\partial z} - \zeta_x * \frac{\partial H_z}{\partial x}\right) \tag{13}$$

$$\varepsilon_0 \frac{\partial E_z}{\partial t} + J_z = \left(\frac{1}{k_x}\frac{\partial H_y}{\partial x} - \frac{1}{k_y}\frac{\partial H_x}{\partial y}\right) + \left(\zeta_x * \frac{\partial H_y}{\partial x} - \zeta_y * \frac{\partial H_x}{\partial y}\right) \tag{14}$$

$$-\mu_0 \frac{\partial H_x}{\partial t} = \left(\frac{1}{k_y}\frac{\partial E_z}{\partial y} - \frac{1}{k_z}\frac{\partial E_y}{\partial z}\right) + \left(\zeta_y * \frac{\partial E_z}{\partial y} - \zeta_z * \frac{\partial E_y}{\partial z}\right) \tag{15}$$

$$-\mu_0 \frac{\partial H_y}{\partial t} = \left(\frac{1}{k_z}\frac{\partial E_x}{\partial z} - \frac{1}{k_x}\frac{\partial E_z}{\partial x}\right) + \left(\zeta_z * \frac{\partial E_x}{\partial z} - \zeta_x * \frac{\partial E_z}{\partial x}\right) \tag{16}$$

$$-\mu_0 \frac{\partial H_z}{\partial t} = \left(\frac{1}{k_x}\frac{\partial E_y}{\partial x} - \frac{1}{k_y}\frac{\partial E_x}{\partial y}\right) + \left(\zeta_x * \frac{\partial E_y}{\partial x} - \zeta_y * \frac{\partial E_x}{\partial y}\right) \tag{17}$$

where * denotes a convolution and:

$$k_x = \begin{cases} 1 + \left(k_{x,\max} - 1\right)\left(\frac{x}{d}\right)^m, & 0 \le x \le d \\ 1, & \text{otherwise} \end{cases} \tag{18}$$

$$\zeta_x = -\frac{\sigma_x}{\varepsilon_0 k_x^2} e^{-\left(\frac{\sigma_x}{\varepsilon_0 k_x} + \frac{a_x}{\varepsilon_0}\right)t} u(t) \tag{19}$$

$$\sigma_x = \sigma_{\max}\left(\frac{x}{d}\right)^m \tag{20}$$

$$\sigma_{\max} = -\frac{(m+1)\ln R}{2\eta_0 d}, \quad \eta_0 = \sqrt{\frac{\mu_0}{\varepsilon_0}} \tag{21}$$

$$a_x = \begin{cases} a_{x,\max}\left(\frac{d-x}{d}\right)^{m_a}, & 0 \le x \le d \\ 0, & \text{otherwise} \end{cases} \tag{22}$$

where d is the thickness of the PML, $u(t)$ is the unit step function, R is the desired reflection error which the optimal choice for a ten-layer PML is $R = e^{-16}$, m_a is the scaling order where $2 \le m_a \le 3$ and m, $k_{x,\max}$ and $a_{x,\max}$ are PML constants in the range of, $1 < k_{x,\max} < 2, 3 \le m \le 4$ and $0.1 \le a_{x,\max} \le 0.3$ (Taflove and Hagness 2005). Similar equations have been defined for k_y, k_z, ζ_y and ζ_z.

For the lossless case, the guided modes in PCFs have the term of $\exp(-j\beta z)$, where β is the longitudinal propagation constant. Therefore the z-derivatives can be replaced by $-j\beta$. Thus, instead of three-dimensional mesh grids, just two dimensional ones are used for the FDTD algorithm. Following a standard Yee scheme (Yee 1966), Eq. 12 is discretized in time and space as:

$$\begin{aligned} &\varepsilon_0 \left(\frac{E_x\big|_{i+1/2,j}^{n+1/2} - E_x\big|_{i+1/2,j}^{n-1/2}}{\Delta t}\right) + J_x\big|_{i+1/2,j}^{n} \\ &= \left[\frac{H_z\big|_{i+1/2,j+1/2}^{n} - H_z\big|_{i+1/2,j-1/2}^{n}}{k_{y_j}\Delta y} + \frac{j\beta H_y\big|_{i+1/2,j}^{n}}{k_{z_k}}\right. \\ &\quad \left. + \psi_{E_{x,y}}\big|_{i+1/2,j}^{n} - \psi_{E_{x,z}}\big|_{i+1/2,j}^{n}\right] \end{aligned} \tag{23}$$

where (Taflove and Hagness 2005):

$$\psi_{E_{x,y}}\big|^{n}_{i+1/2,j} = b_{y_j}\ \psi_{E_{x,y}}\big|^{n-1}_{i+1/2,j} + c_{y_j}\left(\frac{H_z|^{n}_{i+1/2,j+1/2} - H_z|^{n}_{i+1/2,j-1/2}}{\Delta y}\right) \tag{24}$$

$$\psi_{E_{x,z}}\big|^{n}_{i+1/2,j} = b_{z_k}\ \psi_{E_{x,z}}\big|^{n-1}_{i+1/2,j} - c_{z_k} j\beta\ H_y\big|^{n}_{i+1/2,j} \tag{25}$$

$$b_{y_j} = e^{-\left(\frac{\sigma_y}{\varepsilon_0 k_y} + \frac{a_y}{\varepsilon_0}\right)\Delta t} \tag{26}$$

$$c_{y_j} = \frac{\sigma_y\left(b_{y_j} - 1\right)}{\sigma_y k_y + k_y^2 a_y} \tag{27}$$

The same equations can be derived for b_{z_k} and c_{z_k}.

Then from Eq. 9 we have:

$$\left(\frac{J^{\pm}_{k_x}\Big|^{n+1/2}_{i+1/2,j} - J^{\pm}_{k_x}\Big|^{n-1/2}_{i+1/2,j}}{\Delta t}\right) \pm j\omega_k\left(\frac{J^{\pm}_{k_x}\Big|^{n+1/2}_{i+1/2,j} + J^{\pm}_{k_x}\Big|^{n-1/2}_{i+1/2,j}}{2}\right)$$
$$= \frac{\varepsilon_0}{2}\ b_{k_x}\big|_{i+1/2,j}\ \omega_k^2\left(\frac{E_x|^{n+1/2}_{i+1/2,j} + E_x|^{n-1/2}_{i+1/2,j}}{2}\right) \tag{28}$$

By re-arranging and simplifying Eq. 28, one can get:

$$J^{\pm}_{k_x}\Big|^{n+1/2}_{i+1/2,j} = k_k^{\pm}\ J^{\pm}_{k_x}\Big|^{n-1/2}_{i+1/2,j} + \beta^{\pm}_{k_x}\Big|_{i+1/2,j}\left(\frac{E_x|^{n+1/2}_{i+1/2,j} + E_x|^{n-1/2}_{i+1/2,j}}{2}\right) \tag{29}$$

for $k = 1$ and 2, where:

$$k_k^{\pm} = \frac{2 \mp j\omega_k\Delta t}{2 \pm j\omega_k\Delta t} \tag{30}$$

$$\beta^{\pm}_{k_x}\Big|_{i+1/2,j} = \frac{\varepsilon_0\ b_{k_x}\big|_{i+1/2,j}\ \omega_k^2\Delta t}{2 \pm j\omega_k\Delta t} \tag{31}$$

To improve the convergence and the accuracy of our FDTD method, we have used a modified conformal FDTD in which the coefficients of the refractive index of silica, b_{k_x}, b_{k_y} and b_{k_z}, have been averaged for the cells around the medium circular boundary. For example, $b_{k_x} = f_x b_k$, where f_x is the fraction of the cell occupied by the fused silica in the x direction. The detailed computation methods of f_x, f_y and f_z are given in Appendix A.

Equation 29 is an explicit update equation for $J^{\pm}_{k_x}$. The term $J_x|^{n}_{i+1/2,j}$ in Eq. 23 is also evaluated as:

$$J^{\pm}_{k_x}\Big|^{n}_{i+1/2,j} = \left(\frac{J^{\pm}_{k_x}\Big|^{n-1/2}_{i+1/2,j} + J^{\pm}_{k_x}\Big|^{n+1/2}_{i+1/2,j}}{2}\right)$$
$$= \frac{1}{2}\left(1 + k_k^{\pm}\right)\ J^{\pm}_{k_x}\Big|^{n-1/2}_{i+1/2,j} + \frac{\beta^{\pm}_{k_x}\Big|_{i+1/2,j}}{4}\left(E_x|^{n+1/2}_{i+1/2,j} + E_x|^{n-1/2}_{i+1/2,j}\right) \tag{32}$$

and from Eq. 8, we have:

$$J_x|^{n}_{i+1/2,j} = \frac{1}{2}\sum_{k=1}^{2}\left[\left(1+k_k^{+}\right) J_{k_x}^{+}\Big|^{n-1/2}_{i+1/2,j}\right] + \frac{1}{2}\sum_{k=1}^{2}\left[\left(1+k_k^{-}\right) J_{k_x}^{-}\Big|^{n-1/2}_{i+1/2,j}\right] + \frac{\left(E_x|^{n+1/2}_{i+1/2,j} + E_x|^{n-1/2}_{i+1/2,j}\right)}{4}\sum_{k=1}^{2}\left[\beta_{k_x}^{+}\big|_{i+1/2,j} + \beta_{k_x}^{-}\big|_{i+1/2,j}\right] \quad (33)$$

After substituting Eq. 33 in Eq. 23, an explicit update equation for x-component of the electric field is obtained as:

$$E_x|^{n+1/2}_{i+1/2,j} = C_{a,E_x}\big|_{i+1/2,j} E_x|^{n-1/2}_{i+1/2,j} + C_{b,E_x}\big|_{i+1/2,j}\left[\frac{H_z|^{n}_{i+1/2,j+1/2} - H_z|^{n}_{i+1/2,j-1/2}}{k_{y_j}\Delta y} + \frac{j\beta H_y|^{n}_{i+1/2,j}}{k_{z_k}} + \psi_{E_{x,y}}|^{n}_{i+1/2,j} - \psi_{E_{x,z}}|^{n}_{i+1/2,j} - \frac{1}{2}\sum_{k=1}^{2}\left[\left(1+k_k^{+}\right) J_{k_x}^{+}\Big|^{n-1/2}_{i+1/2,j} + \left(1+k_k^{-}\right) J_{k_x}^{-}\Big|^{n-1/2}_{i+1/2,j}\right]\right] \quad (34)$$

where:

$$C_{a,E_x}\big|_{i+1/2,j} = \frac{\varepsilon_0 - I_x|_{i+1/2,j}\,\Delta t}{\varepsilon_0 + I_x|_{i+1/2,j}\,\Delta t} \quad (35)$$

$$C_{b,E_x}\big|_{i+1/2,j} = \frac{\Delta t}{\varepsilon_0 + I_x|_{i+1/2,j}\,\Delta t} \quad (36)$$

$$I_x|_{i+1/2,j} = \frac{1}{4}\sum_{k=1}^{2}\left[\beta_{k_x}^{+}\big|_{i+1/2,j} + \beta_{k_x}^{-}\big|_{i+1/2,j}\right] \quad (37)$$

which the update equation for $J_{k_x}^{\pm}\Big|^{n-1/2}_{i+1/2,j}$ is Eq. 29. The same equations can be derived for the y and z-components of the electric field.

Also, Eq. 15 is discretized in time and space to derive update equation for the x-component of the magnetic fields as follows (Taflove and Hagness 2005):

$$H_x|^{n+1}_{i,j+1/2} = H_x|^{n}_{i,j+1/2} - \frac{\Delta t}{\mu_0}\left[\frac{E_z|^{n+1/2}_{i,j+1} - E_z|^{n+1/2}_{i,j}}{k_{y_{j+1/2}}\Delta y} + \frac{j\beta E_y|^{n+1/2}_{i,j+1/2}}{k_{z_{k+1/2}}} + \psi_{H_{x,y}}|^{n+1/2}_{i,j+1/2} - \psi_{H_{x,z}}|^{n+1/2}_{i,j+1/2}\right] \quad (38)$$

$$\psi_{H_{x,y}}|^{n+1/2}_{i,j+1/2} = b_{y_{j+1/2}}\psi_{H_{x,y}}|^{n-1/2}_{i,j+1/2} + c_{y_{j+1/2}}\left(\frac{E_z|^{n+1/2}_{i,j+1} - E_z|^{n+1/2}_{i,j}}{\Delta y}\right) \quad (39)$$

$$\psi_{H_{x,z}}|^{n+1/2}_{i,j+1/2} = b_{z_{k+1/2}}\,\psi_{H_{x,z}}|^{n-1/2}_{i,j+1/2} - c_{z_{k+1/2}} j\beta\; E_y|^{n+1/2}_{i,j+1/2} \quad (40)$$

Again the same equations can be derived for the y and z-components of the magnetic field.

3 Results and discussions

In this project, we have used the FDTD method to simulate the performance and calculate the parameters of the PCFs, by our FORTRAN code with 50000 time step. The computer used in this simulation was P4 3.20 GHz (Dual Core) which had 2 GB of RAM (Dual channel). Computation memory for our FDTD method actually depends on the operating wavelength. For example, for the third telecommunication window wavelength, our FDTD codes consume about 400 Mbytes of memory and takes about 45 minutes to calculate n_{eff} for each selected wavelength. It is to be noted that the time and memory consumption increase with the decrease of wavelength. In all the numerical simulations of this paper, a ten-layer CPML has been used. Also, the operating wavelength has been assumed to be $\lambda = 1.55\mu\text{m}$, $\Delta x = \Delta y = \Delta$ and $\Delta t = \Delta/(2c)$, where c is the speed of light in vacuum. For evaluation of our algorithm, first we analyzed a conventional standard step index fiber with core radius of 4μm and core and cladding refractive indices, n_1 and n_2 of 1.460 and 1.455, respectively. Normalized propagation constant $b = (n_{\text{eff}}^2 - n_2^2)/(n_1^2 - n_2^2)$ (where $n_{\text{eff}} = \beta/k_0$ and $k_0 = 2\pi/\lambda$) of this fiber has been derived by analytical and our FDTD methods. In analytical method b is computed by solving the characteristic equation of fiber. Characteristic equation of fiber for linearly polarized (LP_{lm}) modes in weakly guiding conditions is defined as (Cherin 1983):

$$U\frac{J_1(U)}{J_0(U)} = W\frac{K_1(W)}{K_0(W)}, \quad l = 0 \tag{41}$$

and

$$U\frac{J_{l-1}(U)}{J_l(U)} = -W\frac{K_{l-1}(W)}{K_l(W)}, \quad l \geq 1 \tag{42}$$

where:

$$U = a(k_0^2 n_1^2 - \beta^2)^{1/2}, \quad W = a(\beta^2 - k_0^2 n_2^2)^{1/2} \tag{43}$$

where a is the core radius of the fiber, $J_l(U)$ is the Bessel's function of the first kind and $K_l(U)$ is the modified Bessel's function of the second kind, of order l. By employing the fiber normalized frequency $V = (U^2 + W^2)^{1/2} = k_0 a(n_1^2 - n_2^2)^{1/2}$, one can write:

$$b = \frac{n_{\text{eff}}^2 - n_2^2}{n_1^2 - n_2^2} = \frac{k_0^2 a^2\left(\frac{\beta^2}{k_0^2} - n_2^2\right)}{k_0^2 a^2(n_1^2 - n_2^2)} = \frac{W^2}{V^2} \tag{44}$$

thus, $W = V\sqrt{b}$ and $U = \sqrt{V^2 - W^2} = V\sqrt{1-b}$. Substituting W and U into Eqs. 41 and 42 yields:

$$V\sqrt{1-b}\frac{J_1(V\sqrt{1-b})}{J_0(V\sqrt{1-b})} = V\sqrt{b}\frac{K_1(V\sqrt{b})}{K_0(V\sqrt{b})} \quad l = 0 \tag{45}$$

and

$$V\sqrt{1-b}\frac{J_{l-1}(V\sqrt{1-b})}{J_l(V\sqrt{1-b})} = -V\sqrt{b}\frac{K_{l-1}(V\sqrt{b})}{K_l(V\sqrt{b})} \quad l \geq 1 \tag{46}$$

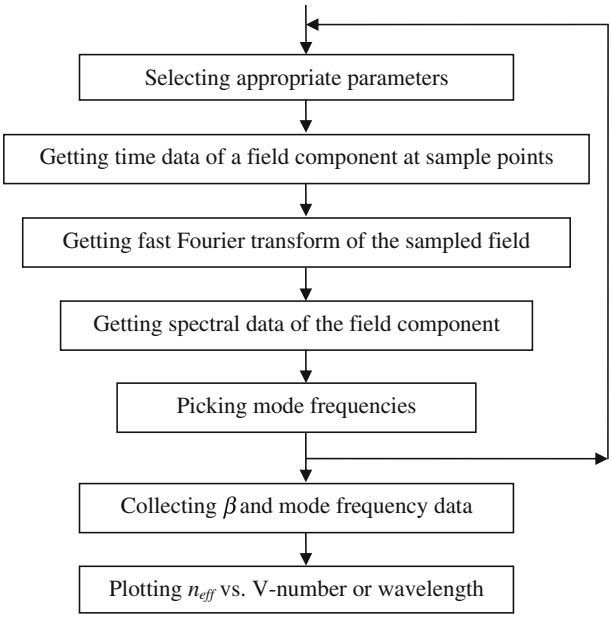

Fig. 2 Flow chart of the FDTD algorithm used in this paper

For the first and second order modes of the fiber (LP_{01} and LP_{11}), b is derived for different values of V, by solving Eqs. 45 and 46. Also effective refractive index of fiber is defined as:

$$n_{\text{eff}} = \frac{\beta}{k_0} = \left[n_2^2 + b\left(n_1^2 - n_2^2\right)\right]^{1/2} \tag{47}$$

In the numerical calculation of b, n_{eff} can be computed by getting the spectral information of the electromagnetic fields. This can be achieved by getting fast Fourier transform of the electromagnetic fields (Navarro et al. 1991; Jacquin et al. 2000; Qiu and He 2000). In fact, by getting fast Fourier transform, we transform all the fields from time domain to frequency domain. The numerical procedure of computing n_{eff} by the FDTD algorithm is shown in the flow chart of Fig. 2. According to the flow chart of the FDTD algorithm, appropriate parameters such as λ, Δx, Δt, time step and so on are selected first. Then the electromagnetic fields are sampled in each time step in different arrays. Next, the Fast Fourier Transforms (FFTs) of the sample fields are derived. Now, if the absolute values of the data of the FFT arrays are plotted versus frequency, there will be some peaks in the graph. The frequency of the first peak is the frequency of the fundamental mode of the fiber and the $n_{\text{eff}} = \beta/k_0$ can be derived for the selected wavelength (Taflove and Hagness 2005). Therefore, in each running of the program, n_{eff} is determined for a specific wavelength.

By calculation of n_{eff} for different values of normalized frequency, b can be simply derived by Eq. 44. As shown in Fig. 3, the normalized propagation constant (b) of the first and second order modes, computed with our FDTD and analytical methods demonstrate a wonderful agreement.

Then, we analyzed a PCF with the structure of Fig. 1, where Λ is 2.3μm and d is 1μm. The contour plot of the E_x of the fundamental mode of the selected PCF is shown in Fig. 4.

Next, we calculated the material and chromatic dispersions of the fundamental mode, in PCFs. Material and chromatic dispersions are, respectively, defined as (Brechet et al. 2000;

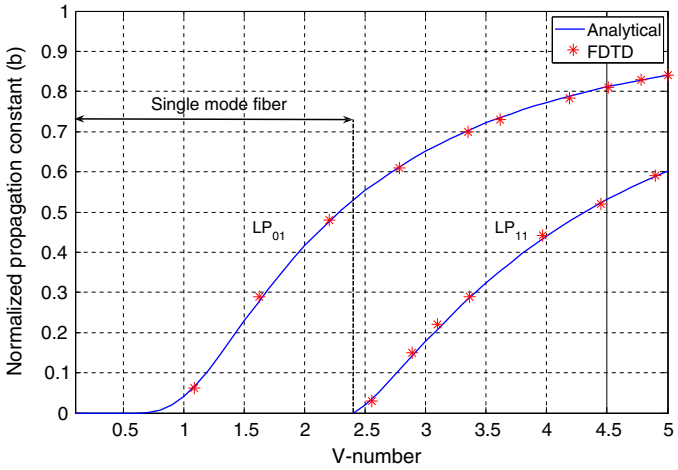

Fig. 3 Variations of the normalized propagation constant, b, of the first and second order linearly polarized modes of a conventional step index fiber versus V-number, derived by analytical and FDTD method

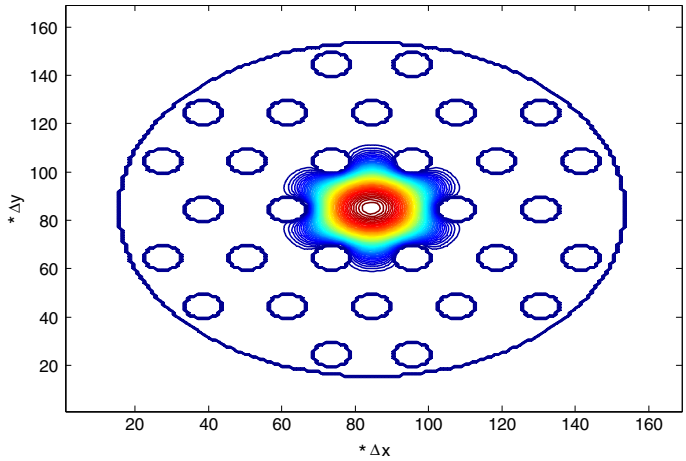

Fig. 4 Contour plot of E_x of the fundamental mode of the PCF of Fig. 1 at $\lambda = 1.55\mu m$

Laegsgaard et al. 2003; Sang et al. 2005):

$$D_m = -\frac{\lambda}{c}\frac{d^2 n_{\text{silica}}}{d\lambda^2}$$
$$D = -\frac{\lambda}{c}\frac{d^2 n_{\text{eff}}}{d\lambda^2} \tag{48}$$

where n_{eff} is the effective refractive index of PCF.

By calculation of n_{eff}, the PCF chromatic dispersion can be simply computed by Eq. 48 for different wavelengths. Also, by using Eq. 48, waveguide dispersion in PCFs can be computed by calculation of n_{eff} with the previous FDTD method, assuming $n_{\text{silica}} = 1.45$ for all wavelengths. As shown in Fig. 5, the material dispersion of PCFs is easily calculated from Sellmeier relation (Eq. 3), using Eq. 48.

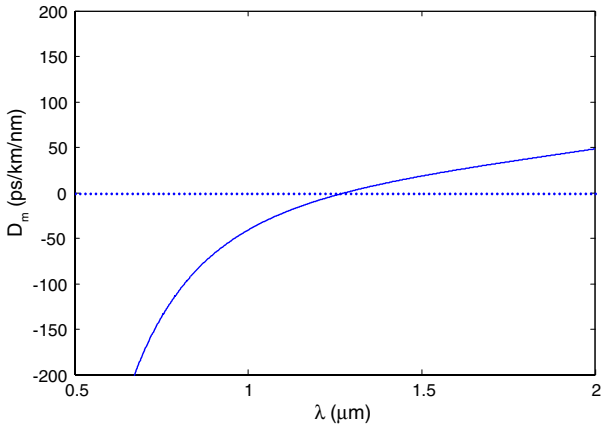

Fig. 5 Material dispersion of the PCFs as a function of wavelength

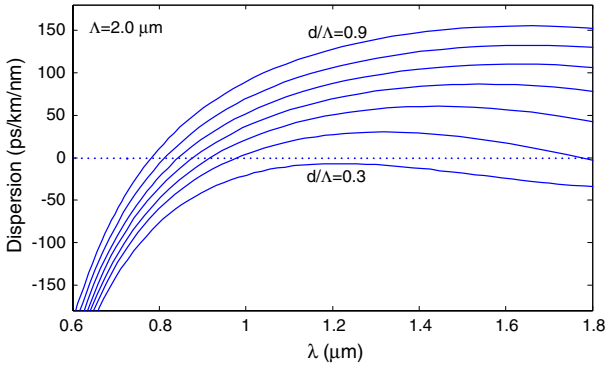

Fig. 6 Chromatic dispersion of the PCFs as a function of wavelength for $\Lambda = 2.0\mu m$

Figures 6, 7 and 8 show the chromatic dispersion properties of PCFs with different geometrical parameters such as lattice pitch (Λ) and hole diameter (d) as a function of wavelength. The derived results in these Figures are in good agreement with those of obtained by FEM (Saitoh and Koshiba 2002; Koshiba and Saitoh 2004). As all the figures show, the chromatic dispersion profile of holey fibers can easily be controlled by varying the hole diameter, the lattice pitch and consequently their zero dispersion wavelength can be shifted. We also see that it is possible to have holey fibers with flattened dispersion behavior. Contrary to the conventional optical fibers, it is possible to easily control the PCFs chromatic dispersion behavior by changing their geometrical parameters.

As shown in Fig. 8, the dispersion of the holey fiber with $\frac{d}{\Lambda} = 0.3$ and $\Lambda = 3.0\mu m$, is close to the material dispersion of pure silica. This is due to the fact that when Λ increases and $\frac{d}{\Lambda}$ decreases, consequently the air to silica ratio decreases and most of the fiber is silica, so the material dispersion overcomes the waveguide one. On the contrary, when the hole diameter to pitch ratio increases, the waveguide dispersion overcomes the material one.

It is also possible to have two zero dispersion wavelengths, by changing the geometrical parameters of photonic crystal fibers. These PCFs which possess a small lattice pitch, have one zero dispersion wavelength in the visible region, as shown in Fig. 9.

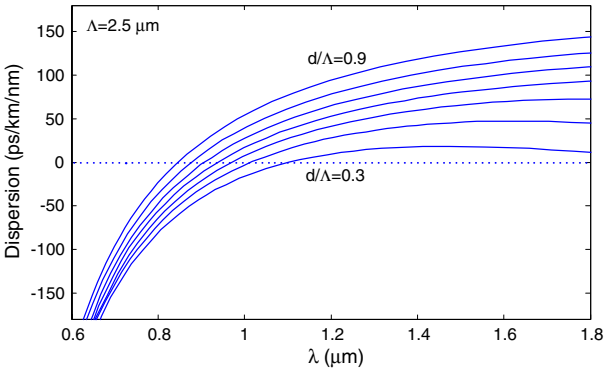

Fig. 7 Chromatic dispersion of the PCFs as a function of wavelength for $\Lambda = 2.5\mu m$

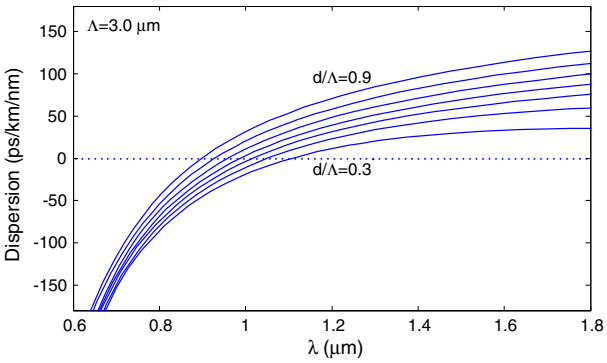

Fig. 8 Chromatic dispersion of the PCFs as a function of wavelength for $\Lambda = 3.0\mu m$

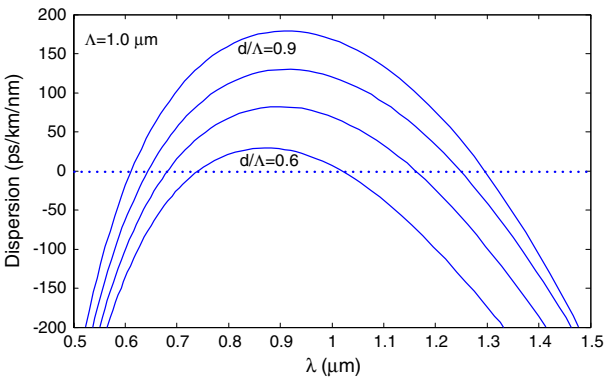

Fig. 9 Chromatic dispersion of the PCFs as a function of wavelength for $\Lambda = 1.0\mu m$

4 Conclusion

In this paper, we have analyzed the index-guiding PCF with inclusion of material and chromatic dispersion by our proposed FDTD algorithm which its accuracy and validity was shown by applying it to the conventional step index fibers. With our FDTD software, the electric field contour of the fundamental mode of PCF was demonstrated. We have also used a modified conformal FDTD method for convergence and accuracy of our algorithm. The mathematical algorithm in developing the methodology is thorough and straightforward compared to FEM.

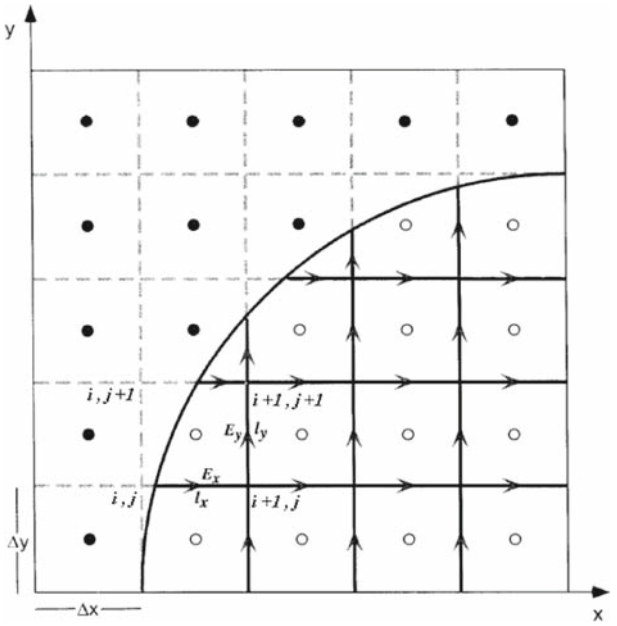

Fig. 10 Cross-sectional view of quarter of a circular cylindrical air hole

The requirement for the computer memory is moderate and our presented method takes lower time compared to the other numerical methods and the results show a great accuracy.

Obviously, our extended FDTD algorithm is capable to be applied to any other PCFs with arbitrary refractive index profile.

Acknowledgements The authors would like to express their thanks to Iran Telecommunication Research Center (ITRC) for the financial support of this project.

Appendix A

Cross sectional pattern of a quarter of a typical air hole of Fig. 1, has been shown in Fig. 10. As mentioned before, the position-dependent parameters ($b_{k_x}|_{i+1/2,j}$, $b_{k_y}|_{i,j+1/2}$ and $b_{k_z}|_{i,j}$) of Eq. 31 is defined as follows:

1. In the fused silica matrix of the PCF, they are equal to b_k.
2. In the air holes matrix of the PCF, they are zero.
3. For the cells around the circular boundaries, they are averaged as:

$$b_{k_x}|_{i+1/2,j} = f_x|_{i+1/2,j}\, b_k, \quad b_{k_y}|_{i,j+1/2} = f_y|_{i,j+1/2}\, b_k, \quad b_{k_z}|_{i,j} = f_z|_{i,j}\, b_k$$

where $f_x|_{i+1/2,j}$, $f_y|_{i,j+1/2}$ and $f_z|_{i,j}$ are the fraction of the cell occupied by the fused silica in the x, y and z direction, respectively.

For example, for the grid point of i, j of Fig. 10, $f_x|_{i+1/2,j} = \frac{\Delta x - l_x}{\Delta x}$ because only this fraction of the cell has been occupied by the fused silica in the x direction. Also, $f_y|_{i,j+1/2} = f_z|_{i,j} = 1$ and it is due to the fact that all the cell has been occupied by the fused silica in

the y and z directions. By the same method, the position-dependent parameters are defined for all the FDTD mesh grids.

References

Brechet, F., Marcou, J., Pagnoux, D., Roy, P.: Complete analysis of the characteristics of propagation into photonic crystal fibers, by the finite element method. Opt. Fiber Technol. **6**, 181–191 (2000). doi:10.1006/ofte.1999.0320

Cherin, A.H.: An Introduction to Optical Fibers. Bell Lab. (1983)

Jacquin, O., Benyattou, T., Desieres, Y., Orobtchouk, R., Cachard, A., Benech, P.: Diffraction effects in guided photonic band gap structure. Opt. Quantum Electron. **32**, 935–945 (2000). doi:10.1023/A:1007087016802

Jiang, W., Shen, L., Chen, D., Chi, H.: An extended FDTD method with inclusion of material dispersion for the full-vectorial analysis of photonic crystal fibers. J. Lightwave Technol. **24**, 4417–4423 (2006). doi:10.1109/JLT.2006.883651

Koshiba, M., Saitoh, K.: Applicability of classical optical fiber theories to holey fibers. Opt. Lett. **29**, 1739–1741 (2004). doi:10.1364/OL.29.001739

Laegsgaard, J., Bjarklev, A., Libori, S.E.B.: Chromatic dispersion in photonic crystal fibers: Fast and accurate scheme for calculation. J. Opt. Soc. Am. B **20**, 443–448 (2003). doi:10.1364/JOSAB.20.000443

Malitson, L.H.: Interspecimen comparison of the refractive index of fused silica. J. Opt. Soc. Am. **55**, 1205–1208 (1965). doi:10.1364/JOSA.55.001205

Navarro, A., Nuhez, M.J., Martin, E.: Study of TE and TM modes in dielectric resonators by a finite difference time domain method coupled with the discrete Fourier transform. IEEE Trans. Microw. Theory Tech. **39**, 14–17 (1991). doi:10.1109/22.64599

Qiu, M., He, S.: Numerical method for computing defect modes in two-dimensional photonic crystals with dielectric or metallic inclusions. Phys. Rev. B Condens. Matter **61**, 12871–12876 (2000). doi:10.1103/PhysRevB.61.12871

Saitoh, K., Koshiba, M.: Full-vectorial imaginary-distance beam propagation method based on a finite element scheme: application to photonic crystal fibers. IEEE J. Quantum Electron. **38**, 927–933 (2002). doi:10.1109/JQE.2002.1017609

Sang, X., Chu, P.L., Yu, C.: Applications of nonlinear effects in highly nonlinear photonic crystal fiber to optical communications. Opt. Quantum Electron. **37**, 965–994 (2005). doi:10.1007/s11082-005-8338-4

Taflove, A., Hagness, S.C.: Computational Electrodynamics: The Finite-Difference Time-Domain Method. Boston: Boston, Artech House (2005)

Yee, K.S.: Numerical solution of initial boundary value problems involving Maxwell's equations in isotropic media. IEEE Trans. Antennas Propag. **14**, 302–307 (1966). doi:10.1109/TAP.1966.1138693